

An improved 1-D thermal model of parabolic trough receivers: Consideration of pressure drop and kinetic energy loss effects

Yassine Demagh*

LESEI, Mechanical Department, University of Batna 2, 05000 Batna, Algeria

(Received March 24, 2020, Revised November 28, 2020, Accepted December 3, 2020)

Abstract. In this study, the first law of thermodynamics was used to establish a one-dimensional (1-D) thermal model for parabolic trough receiver (PTR) taking into account the pressure drop and kinetic energy loss effects of the heat transfer fluid (HTF) flowing inside the absorber tube. The validation of the thermal model with data from the SEGS-LS2 solar collector-test showed a good agreement, which is consistent with the previously established models for the conventional straight and smooth (CSS) receiver where the effects of pressure drop and kinetic energy loss were neglected. Based on the developed model and code, a comparative study of the newly designed parabolic trough S-curved receiver versus the CSS receiver was conducted and solar unit's performances were analyzed. Without any supplementary devices, the S-curved receiver enhances the performance of the parabolic trough module, with a maximum of 0.16% compared to CSS receiver with the same sizes and mass flow rates. Thermal losses were reduced by 7% due to the decrease in the temperature of the outer surface of the receiver tube. In addition, it has been shown that from a mass flow rate of 9.5 kg/s the heat losses of the S-curved receiver remain unchanged despite the improvement in the heat transfer rate.

Keywords: 1-D thermal model; conventional straight receiver; kinetic energy loss; pressure drop; S-curved receiver

1. Introduction

With various domestic and industrial applications, parabolic trough collector (PTC) is the most mature concentrating technology for the production of usable energy from the direct irradiation of the sun, Fuqiang *et al.* (2017). A number of studies dealing with this technology have shown that 1-D mathematical models that take into account almost all thermal exchanges are a powerful tool for assessing the thermal performance of the CSS receivers. Forristall (2003) proposed 1-D and 2-D thermal models (radial and longitudinal), respectively for short and long receivers, where thermal conduction through the absorber wall was assumed. After validation of the results with experimental data from Dudley *et al.* (1994), many recommendations and suggestions were proposed to improve the parabolic trough solar receiver (PTR) performance. Gong *et al.* (2010) combined, through Fluent-CFD software, the 1-D radial model of Forristall (2003) with a 3-D end model to identify the influence of the receiver ends on the total heat losses. No modifications had been made to the original 1-D radial model of Forristall (2003). Padilla *et al.* (2011) presented a heat transfer analysis of a

*Corresponding author, Ph.D., E-mail: y.demagh@univ-batna2.dz

PTR based on a longitudinal one-dimensional thermal model. A comprehensive analysis of the radiation heat transfer was implemented to take into account the radiative heat exchange between adjacent surface segments (absorber-envelope, and envelope-envelope), neglected in previous studies. Kalogirou (2012) developed a detailed thermal model to analyse the solar collector installed in the Archimedes Solar Energy Laboratory (Cyprus University of Technology) for two operating conditions: a vacuum annulus and an annular space containing air. Lu *et al.* (2013) and Cheng *et al.* (2015) investigated effects of the non-uniform distribution of the solar radiation on the glass envelope and the absorber tube using a 1-D radial thermal model; the originality of these studies was to subdivide the PTR in two parts to assume different solar radiation for each of them. Liang *et al.* (2015) established a 1-D model for a PTC under different assumptions and conditions based on the differential form of the energy equation. After validation by comparison with models established previously, they concluded that the efficiency could increase with a longer absorber rather than with a short absorber. Moreover, the authors reported that the heat conduction through the wall of the glass envelope and the absorber tube can be neglected. Huang *et al.* (2016) developed a thermal model of the solar trough system with vacuumed receiver based on energy balance. They concluded that taking into account the direct transmission by the glass envelope of long wave radiation improve the prediction accuracy of the radiation model. On the basis of a 1-D model analysis, Guo *et al.* (2016) highlighted the existence of an optimal mass flow rate of HTF for exergy efficiency. Results showed that the thermal efficiency and exergy efficiency have opposite changing tendencies under some conditions. The authors concluded that the selection of evaluation criteria is crucial to the performance optimization of solar receiver system. The assumption that the pressure drops and kinetic energy losses being negligible was assumed by all of the above mentioned studies.

The main challenge for the PTC technology is to achieve a more efficient application with the minimum investment, which should be possible by improving the rate of heat transfer per unit area of the solar receiver tube. Among different techniques to achieve higher thermal efficiency, the publications (Kumar and Reddy 2009, Muñoz *et al.* 2011, Cheng *et al.* 2012, Wang *et al.* 2013, Ghadirijafarbeigloo *et al.* 2014, Mwesigye *et al.* 2014, Reddy *et al.* 2015, Kalidasan *et al.* 2016, Fuqiang *et al.* 2016, Gong *et al.* 2017 and Huang *et al.* 2017) reported some evidence on the insertion of additional components into the absorber tube. The most studied insert configurations include: fins, vortex generators, metal foams, twisted-tapes and perforated plates. However, all the works cited above concede that the increase of the overall performances of receiver designs is mainly related to the increased of the receiver part count as compared to the CSS receiver.

Without additional devices, Demagh *et al.* (2015, 2016) proposed a new design of the solar receiver with an S-curved shape of the absorber tube with higher thermal performance as established recently by Bitam *et al.* (2018). The Numerical results showed a better distribution of the reflecting solar radiation on the outer face of the absorber tube and the emergence of vortices inside it, which increases the internal heat exchanges, disturbs the flow, breaks the boundary layer and promotes fluid mixing. Compared to a CSS receiver, the numerical results of Syltherm 800 as HTF revealed an increase of the mean Nusselt number by 63% and the friction factor by 40.8%. The temperature gradient of the absorber wall dropped below 35 K.

As mentioned above, various PTR designs were proposed and several studies were performed with different geometrical parameters, different enhancement techniques, different heat HTFs, different material properties and different operating conditions. However, regarding the variety of the studied parameters, no clear deductions can be made on which one particular design is better than another! The CFD can be used to deal with and solve 3D numerical models, but requires a long time and high memory capacity to achieve computation and establishing comparison. Alternatively,

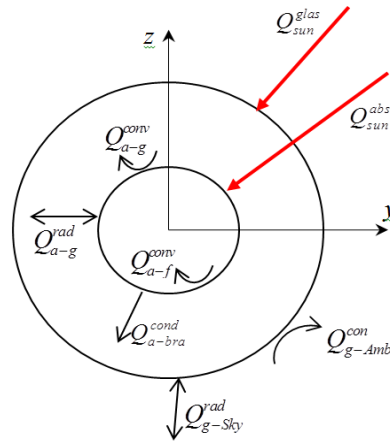


Fig. 1 The receiver cross-sectional view showing heat exchanges

simpler methods like 1-D thermal models, as described in the second paragraph of this section, were found to be sufficient to study CSS receivers by comparing different designs performances.

Unfortunately, none of the models developed to date could be used to study the newly designed absorbers, as declared in Forristall (2003). Because of the improving thermal techniques, the pressure drops and kinetic energy losses through the absorber tube are considerable and may not be neglected, as was the case previously for CSS receiver. Although Forristall (2003) had quoted in his text the correlation of Colebrook for estimating the friction coefficient in smooth and straight tubes; his model never took into account the pressure drop or the kinetic energy losses.

The main objective of this study is to provide an accurate tool to quickly determine the performance and heat loss of newly designed PTRs, developed mainly to improve the heat transfer rate. Unfortunately, these thermal enhancement devices are always accompanied by an increased pressure drop penalty (Kumar and Reddy 2009, Muñoz *et al.* 2011, Cheng *et al.* 2012, Wang *et al.* 2013, Ghadirijafarbigloo *et al.* 2014, Mwesigye *et al.* 2014, Reddy *et al.* 2015, Kalidasan *et al.* 2016, Fuqiang *et al.* 2016, Gong *et al.* 2017 and Huang *et al.* 2017). For this purpose, a detailed 1-D thermal model was established based on the first law of thermodynamics and taking into account the pressure drop and kinetic energy loss effects inside the absorber tube, always neglected in previous studies. Under different PTCs assumptions and details, a simple algorithm to solve the control equations was adopted and an in-house code was developed. The model and code were validated with known experimental data from the literature (Dudley *et al.* 1994). Also, the code was used to perform a comparative study between the newly designed S-curved solar receiver developed by Demagh *et al.* (2015, 2016) and the CSS receiver as presented in Forristall (2003).

2. Mathematic modelling

PTC module includes a parabolic reflector to focus the incident solar radiation on the receiver along the focal line. The heat exchanges on a cross-sectional view of the solar receiver are shown in Fig. 1, while Fig. 2 shows the thermal-electric equivalence model corresponding to the heat exchanges of Fig. 1. The CSS receiver, displayed in Fig. 3 is a straight absorber tube enveloped with a glass tube and with bellows at both ends. To increase the absorption process of the solar

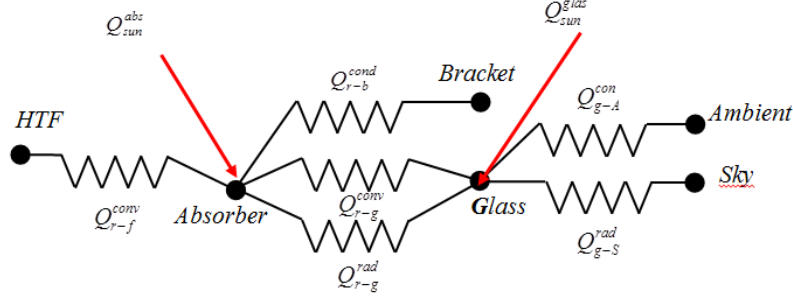


Fig. 2 Thermal-Electric equivalence model

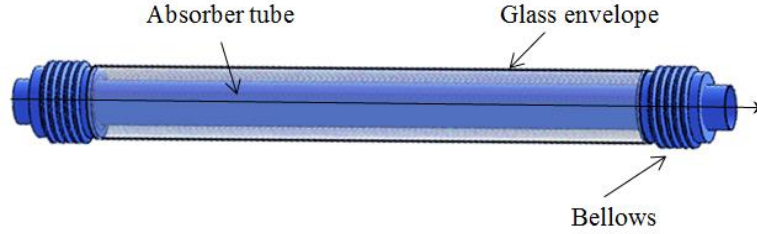


Fig. 3 Conventional smooth and straight PTR

irradiation and reducing thermal radiation losses, absorber tubes are coated with solar selective coatings with high radiation absorptivity in the solar energy spectrum and low thermal emissivity in the long wave energy spectrum. The glass envelope maintains the vacuum created to reduce the convective heat losses and protect the selective coating.

When direct solar insulation (q_{sun}) is reflected by the parabolic mirror onto the receiver it is reduced between 88% and 93% by the mirror reflectivity coefficient (ρ_{mirror}) (Forristall 2003, Liang *et al.* 2015). The mean heat flux of the focused solar energy toward the receiver is computed as ($Q_{sun}^{focused} = \rho_{mirror} \cdot (A_{PTC} \cdot q_{sun})$), (A_{PTC}) being PTC aperture. The glass envelope absorbs the fraction ($Q_{sun}^{glass} = \alpha_{glass} \cdot Q_{sun}^{focused}$). When ($Q_{sun}^{focused}$) is neither absorbed nor reflected by the glass envelope, it passes through and decreases by (τ_{glass}) and hits the absorber tube. Finally, the stainless steel tube absorbs ($Q_{sun}^{absorber}$) and warms up.

The effect of the PTC optical efficiency (η_{opt}) must be taken into account in the energy balance of the absorber tube and the glass envelope. The absorbed mean heat fluxes become

$$\begin{cases} Q_{sun}^{glass} = \eta_{opt} \cdot \rho_{mirror} \cdot \alpha_{glass} \cdot (A_{PTC} \cdot q_{sun}) \\ Q_{sun}^{absorber} = \eta_{opt} \cdot \rho_{mirror} \cdot \tau_{glass} \cdot \alpha_{abs} \cdot (A_{PTC} \cdot q_{sun}) \end{cases} \quad (1)$$

From (Forristall 2003, Dudley *et al.* 1994), the optical efficiency ($\eta_{opt} = \kappa \rho_{clean} \eta_1 \eta_2 \eta_3 \eta_4 \eta_5 \eta_6$) takes into account the effects of: shadowing of the receiver (η_1), tracking error (η_2), mirror geometry error (η_3), dirt on the mirror (η_4), dirt on the receiver (η_5) and others effects (η_6). (ρ_{clean}) is the clean mirror reflectance and eliminating the off-axis cosine effects, the incident angle modifier becomes ($\kappa = 1$). All the optical properties of the SEGS-LS2 are summarised in Table 1.

Table 1 Radiation and optical properties of the SEGS-LS2

Component	Properties
Parabolic trough mirror	$\rho_{mirror} = 0.93$ (Forristall 2003)
Cermet selective coatings	$\alpha_a = 0.92$ (Forristall 2003)
Glass envelope	$\varepsilon_a = 0.327 \cdot 10^{-3} \cdot T_{a,i} - 0.65971 \cdot 10^{-1}$ (Reddy 2015, Bitam 2018)
	$\alpha_g = 0.023, \varepsilon_g = 0.9, \tau_g = 0.935$ (Forristall 2003, Huang 2016)
	$\eta_1 = 0.974, \eta_2 = 0.994, \eta_3 = 0.98, \rho_{clean} = 0.935,$
Effective optical efficiencies	$\eta_4 = \frac{\rho_{mirror}}{\rho_{clean}}, \eta_5 = \frac{(1+\eta_4)}{2}, \eta_6 = 0.96$ (Forristall 2003, Liang 2015)

2.1 Heat transfer modelling

First, and like most heat transfer problems, general assumptions are assumed, namely: zero internal heat generation, negligible viscous dissipation and negligible potential energy change. Secondly, compared to the length of the absorber, the absorber tube and glass envelop thicknesses are small enough to assume uniform temperatures in the wall radial direction, the temperature gradient in the radial direction of the tube walls is zero. This assumption remains in agreement with the study by Liang *et al.* (2015) which reported that the heat conduction from the inner face to outer face of the glass envelope and the absorber tube can be neglected. Thirdly, the working fluid at any cross-section along the longitudinal direction (axis Ox in this study) is expected to be perfectly mixed, so that the HTF temperature is a good approximation uniform at any cross-section of the receiver tube. All assumptions described previously lead to the 1-D model, with $\left(\frac{\partial}{\partial y} = \frac{\partial}{\partial z} = 0\right)$ in this study. Finally, assuming a steady state without work exchange, the generalized first-law statement for an open system would be (Bejan 2013)

$$\sum_{in} \dot{m} \left(u + \frac{P}{\rho} + \frac{V^2}{2} \right) - \sum_{out} \dot{m} \left(u + \frac{P}{\rho} + \frac{V^2}{2} \right) + \dot{Q}_{Net} = 0 \quad (2)$$

$\dot{Q}_{Net} = \sum \dot{Q}_{Inlet} - \sum \dot{Q}_{Outlet}$, is the net heat flux at the system boundary.

The HTF is assumed to be incompressible; the fluid phase internal energy (u) in Eq. (2) is approximated to $(u = c \cdot T)$ (Bejan 2013).

2.2 Discrete equations and domains

The discrete physical model is constructed by dividing the receiver into “N-1” segments (Fig. 4). Each one includes three different subdomains: the glass envelope, the absorber tube and the HTF. With the assumptions stated in the previous section, each subdomain was substituted by a node in the discrete segment, as shown in Figs. 4(a)-(b).

From Figs. 1 and 4, and from Eq. (2), the discrete equations characterising the heat transfer within the glass envelope, absorber tube and HTF would be

$$Q_{Net}|_{g,i} = Q_{sun}^{glas} + Q_{a-g,i}^{conv} + Q_{a-g,i}^{rad} - Q_{g-Amb,i}^{conv} - Q_{g-sky,i}^{rad} = 0 \quad (3a)$$

$$Q_{Net}|_{a,i} = Q_{sun}^{absorber} - Q_{a-g,i}^{conv} - Q_{a-g,i}^{rad} - Q_{a-f,i}^{conv} - Q_{a-bra,i}^{conv} = 0 \quad (3b)$$

$$\dot{m}(c_{i-1}T_{f,i-1} - c_iT_{f,i}) + \dot{m} \left(\frac{\Delta P|_i}{\rho_{f,i}} + \frac{V_{f,i-1}^2 - V_{f,i}^2}{2} \right) + Q_{Net}|_{f,i} = 0 \quad (3c)$$

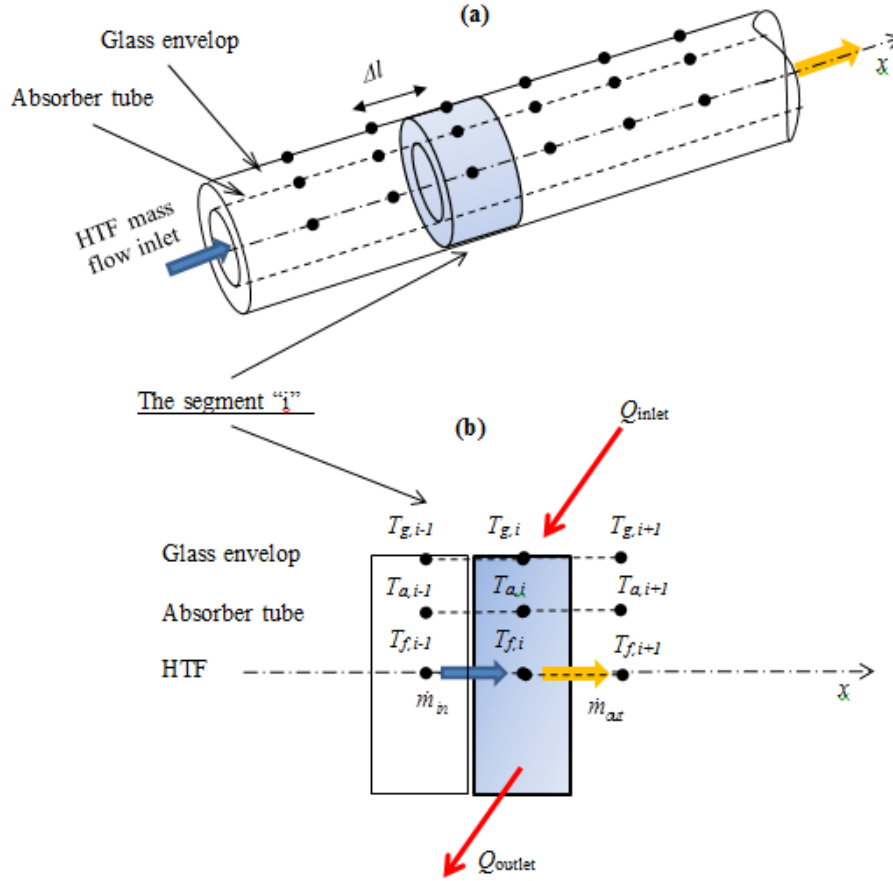


Fig. 4 Discrete physical domain with equal lengths

Where, $T_{f,0} = T_{in}$ is the inlet HTF temperature and $Q_{Net}|_{f,i} = Q_{a-f,i}^{conv}$.

According to the definition of the Moody (or Darcy) friction factor ($f_{inn,i}$) (Incropera *et al.* 2002) the inner pressure drop ($\Delta P|_i$) within a segment “ i ” in the discrete domain (Fig. 4) can be stated as

$$\begin{cases} \Delta P|_i = (P_{i-1} - P_i)|_i = f_{inn,i} \cdot \left(\frac{\Delta l}{D_i}\right) \frac{\bar{\rho}_f \cdot V_{f,i-1}^2}{2} \\ V_{f,i-1} = \frac{\dot{m}_{in}}{\rho_{f,i-1} \cdot A_{cs}} \end{cases} \quad (4)$$

The average HTF density of the HTF subdomain ($\bar{\rho}_f$) is estimated at the arithmetic mean temperature of the inlet and outlet HTF temperatures ($\frac{T_{f,i-1} + T_{f,i}}{2}$) and $V_{f,i-1}$ is the HTF velocity at the inlet of the segment “ i ”, Fig. 4(b).

The various heat fluxes in the set of Eq. (3) were extensively reported in the literature (Forristall 2003, Dudley *et al.* 1994, Gong *et al.* 2010, Padilla *et al.* 2011, Kalogirou 2012, Lu *et al.* 2013, Cheng *et al.* 2015, Liang *et al.* 2015, Huang *et al.* 2016, Guo *et al.* 2016). The Tables 2(a)-2(b)-2(c) recapitulate the various heat flux equations used in the thermal model.

Table 2(a) Convection heat fluxes

Descriptions	Equations
Fluid ↔ Absorber, (Padilla <i>et al.</i> 2011, Huang <i>et al.</i> 2016)	$Q_{a-f,i}^{conv} = h_{a-f,i}^{conv}(\pi \cdot D_{inn}^{abs} \cdot \Delta l)(T_{a,i} - T_{f,i})$ (5a) $h_{a-f,i}^{conv} = \frac{\lambda_{f,i} Nu_i}{D_{inn}^{abs}}$ (5b)
Convection Absorber ↔ Glass (vacuumed in the annulus) pressure < 0.013 Pa (Forristall 2003, Guo <i>et al.</i> 2016)	$Q_{a-g,i}^{conv} = h_{a-g,i}^{conv}(\pi \cdot D_{out}^{abs} \cdot \Delta l)(T_{a,i} - T_{g,i})$ (6a) $h_{a-g,i}^{conv} = \frac{\lambda_{std,i}}{\left(\frac{D_{out}^{abs}}{2 \ln \left(\frac{D_{inn}^{glas}}{D_{out}^{glas}} \right)} + b_{a-g} k_i \left(\left(\frac{D_{out}^{glas}}{D_{inn}^{glas}} \right) + 1 \right) \right)}$ (6b)
	$\begin{cases} b_{a-g} = \frac{(2-a)(9\gamma-5)}{2a(\gamma+1)} \\ k_i = \frac{2.331 \cdot 10^{-20} \cdot T_{a-g,i}}{P_{a-g} \delta^2} \\ T_{a-g,i} [^{\circ}C] = \frac{(T_{a,i} + T_{g,i})}{2} \end{cases}$ (6c)
	Valid for $Ra_{inn}^{glas} < \left(\frac{D_{inn}^{glas}}{(D_{inn}^{glas} - D_{out}^{abs})} \right)^4$ (6d)
Glass ↔ Ambient (forced when there is wind) (Forristall 2003, Guo <i>et al.</i> 2016)	$Q_{g-Amb,i}^{conv} = h_{g-Amb,i}^{conv}(\pi \cdot D_{out}^{glas} \cdot \Delta l)(T_{g,i} - T_{\infty})$ (7a) $h_{g-Amb,i}^{conv} = \frac{Nu_{g-Amb,i} \lambda_{air}}{D_{g,o}}$ (7b) $Nu_{g-Amb,i} = C \cdot Re^m \cdot Pr_{air}^n \cdot \left(\frac{Pr_{air}}{Pr_g} \right)^{0.25}$ (7c)
For more details about C , m and n , the reader is referred to Forristall (2003) and Guo <i>et al.</i> (2016)	

2.3 Numerical procedure

The direct methods cannot be applied to solve the resulting system of equations as it is highly nonlinear and requires iterative methods based on the initial temperature fields $T_{g,i}''$, $T_{a,i}''$ and $T_{f,i}''$. The nonlinearities come mainly from the quadratic term of the radiation heat coefficients and the temperature dependence of the HTF properties such as the Syltherm 800. The thermodynamic and transport properties of the Syltherm 800 are summarised in Table 3 (Delgado-Torres *et al.* 2007).

Based on the system of Eq. (3) and equalities defined in Tables 2(a)-2(b)-2(c), discrete temperatures for each subdomain can be computed as follows

$$T_{a,i} = \frac{\left(\frac{Q_{sun}^{abs}}{\pi \Delta l} \right) + D_{out}^{abs} \cdot (h_{a-g,i}^{conv} + h_{a-g,i}^{rad}) \cdot T_{g,i} + D_{inn}^{abs} \cdot h_{a-f,i}^{conv} T_{f,i}'' + h_{a-bra,i}^{conv} \cdot (T_{amb} + 10)}{D_{out}^{abs} \cdot (h_{a-g,i}^{conv} + h_{a-g,i}^{rad}) + D_{inn}^{abs} \cdot h_{a-f,i}^{conv} + h_{a-bra,i}^{conv}} \quad (11a)$$

$$T_{a,i} = \frac{\left(\frac{Q_{sun}^{abs}}{\pi \Delta l} \right) + D_{out}^{abs} \cdot (h_{a-g,i}^{conv} + h_{a-g,i}^{rad}) \cdot T_{g,i} + D_{inn}^{abs} \cdot h_{a-f,i}^{conv} T_{f,i}'' + h_{a-bra,i}^{conv} \cdot (T_{amb} + 10)}{D_{out}^{abs} \cdot (h_{a-g,i}^{conv} + h_{a-g,i}^{rad}) + D_{inn}^{abs} \cdot h_{a-f,i}^{conv} + h_{a-bra,i}^{conv}} \quad (11b)$$

$$T_{f,i} = \frac{c_{i-1}}{c_i} T_{f,i-1} + \frac{1}{\dot{m} \cdot c_i} \left(\frac{\Delta P|_i}{\rho_{f,i}} + \frac{V_{f,i-1}^2 - V_{f,i}^2}{2} \right) + \frac{h_{a-f,i}^{conv} (\pi \cdot D_{inn}^{abs} \cdot \Delta l) (T_{a,i} - T_{f,i}'')}{\dot{m} \cdot c_i} \quad (11c)$$

Table 2(b) Radiation heat fluxes - (Forristall 2003, Dudley *et al.* 1994, Gong *et al.* 2010, Kalogirou 2012, Lu *et al.* 2013, Cheng *et al.* 2015, Liang *et al.* 2015, Huang *et al.* 2016, Guo *et al.* 2016)

Descriptions		Equations
Radiation	Absorber ↔ Glass	$Q_{a-g,i}^{rad} = h_{a-g,i}^{rad}(\pi \cdot D_{out}^{abs} \cdot \Delta l)(T_{a,i} - T_{g,i})$ (8a)
		$h_{a-g,i}^{rad} = \frac{\sigma(T_{a,i}^2 + T_{g,i}^2)(T_{a,i} + T_{g,i})}{\left(\frac{1}{\varepsilon_{a,o}} + \frac{(1-\varepsilon_{g,i})D_{out}^{abs}}{\varepsilon_{g,i}D_{inn}^{glas}}\right)}$ (8b)
	Glass ↔ Sky	$Q_{g-sky,i}^{rad} = h_{g-sky,i}^{rad}(\pi \cdot D_{out}^{glass} \cdot \Delta l)(T_{g,i} - T_{sky})$ (9a)
		$h_{g-sky,i}^{rad} = \sigma \cdot \varepsilon_g(T_{g,i}^2 + T_{sky}^2)(T_{g,i} + T_{sky})$ (9b)

Table 2(c) Conduction heat flux

Descriptions		Equations
Conduction	Absorber ↔ Bracket	$Q_{a-bra,i}^{conv} = h_{a-bra,i}^{cond} \cdot (T_{base,i} - T_{amb})$ (10a)
	(Forristall 2003, Padilla <i>et al.</i> 2011, Cheng <i>et al.</i> 2015, Liang <i>et al.</i> 2015, Huang <i>et al.</i> 2016)	$h_{a-bra,i}^{cond} = \sqrt{h_{g-a,i}^{conv} \cdot P_{bra} \cdot A_{cs,bra} \cdot \lambda_{bra} \cdot \tanh\left(\sqrt{\frac{h_{g-a,i}^{conv} \cdot P_{bra}}{A_{cs,bra} \cdot \lambda_{bra}}} \cdot f\right)}$ (10b)
		$T_{base,i} = T_{a,i} - 10$ (10c)

Table 3 Thermodynamic and transport properties of the Syltherm 800 (Delgado-Torres *et al.* 2007). The temperature validity range is 373.15 K – 673.15 K

$= a + b \cdot T + c \cdot T^2 + d \cdot T^3 + e \cdot T^4$				
	Density [kg · m ⁻³]	Dynamic viscosity [Pa · s]	Thermal conductivity [W · m ⁻¹ · K ⁻¹]	Specific heat [J · kg ⁻¹ · K ⁻¹]
<i>a</i>	1105.702	0.08486612	0.190021	1107.798
<i>b</i>	-0.4153495	-5.541277 · 10 ⁻⁴	-1.875266 · 10 ⁻⁴	1.708
<i>c</i>	-6.061657 · 10 ⁻⁴	1.388285 · 10 ⁻⁶	-5.753496 · 10 ⁻¹⁰	--
<i>d</i>	--	-1.566003 · 10 ⁻⁹	--	--
<i>e</i>	--	6.672331 · 10 ⁻¹³	--	--

$T_f'' = \frac{T_{f,i}'' + T_{f,i-1}''}{2}$ being the arithmetic mean temperature of the inlet and outlet HTF temperatures from the initial field.

A first loop is used to estimate the new nodal temperatures of the glass envelope ($T_{g,i}$) in Eq. (11a). ($T_{g,i}''$) and ($T_{a,i}''$) are used to start the computing procedures by estimating the convective and radiative heat transfer coefficients, respectively ($h_{a-g,i}^{conv}$, $h_{g-amb,i}^{conv}$) and ($h_{a-g,i}^{rad}$, $h_{a-sky,i}^{rad}$). In the second loop, the glass envelope new nodal temperatures $T_{g,i}$ are used, as well as $T_{a,i}''$ and $T_{f,i}''$, to estimate $T_{a,i}$ in Eq. (11b).

In the last loop, as the HTF inlet temperature is known ($T_{f,0} = T_{in}$), the first guess of the HTF outlet temperature ($T_{f,1}$) of the first subdomain is estimated using ($T_{g,1}$), ($T_{a,1}$) and ($T_{f,1}''$) in Eq. (11c). Therefore, ($T_{f,1}$) is used as inlet temperature to calculate the outlet temperature of the second subdomain, and so on, up to the last HTF temperature at the outlet of the receiver tube. These steps are repeated in an iterative procedure until the error is relatively small ($< 10^{-3}$), and

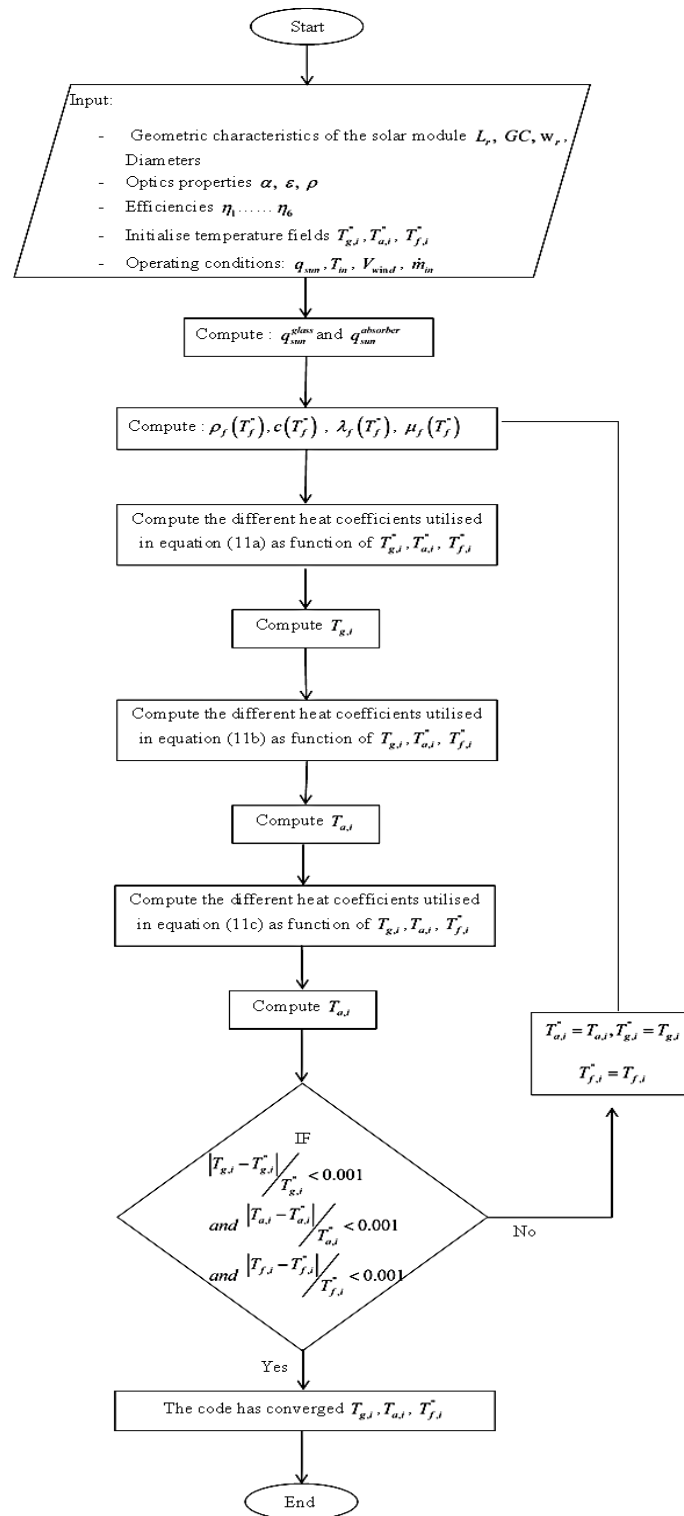


Fig. 5 Simplified numerical model algorithm

each time the initial temperature fields are updated by the new temperatures previously calculated. An algorithm for the numerical procedure is presented in Fig. 5.

2.4 Thermal model and numerical code validation

Accuracy of the thermal model and code are tested by comparison with experimental data from Dudley *et al.* (1994), for the case ‘‘Cermet Selective Coating-Vacuum Annulus’’. To recreate particular operating conditions, the receiver tube of SEGS-LS2 was equipped with a solid plug. Consequently, the annulus Nusselt number ($Nu_{inn,i}$), in Eq. (5b)-Table 2(a), would be expressed as (Padilla *et al.* 2011, Huang *et al.* 2016)

$$\begin{cases} Nu_{inn,i} = (1 - 0.14 \cdot r^{0.6}) \frac{f_{inn,i}(Re_i - 1000)Pr_{f,i}}{1 + 12.7\sqrt{f_{inn,i}/8}(Pr_{f,i}^{2/3} - 1)} \left(\frac{Pr_{f,i}}{Pr_{a,i}} \right) \\ r = \frac{D_{inn}^{abs}}{D_{plug}} \end{cases} \quad (12a)$$

The Darcy friction factor ($f_{inn,i}$) (Eq. (4)) is estimated using the Colebrook’s correlation

$$\begin{cases} \frac{1}{\sqrt{f_{inn,i}}} = -2 \cdot \text{Log} \left(\frac{\varepsilon/D_{inn}}{3.7} + \frac{2.51}{Re_i \sqrt{f_{inn,i}}} \right) \\ 0.5 < Pr_{f,i} < 2000, \quad 2300 < Re_i < 5 \cdot 10^6 \end{cases} \quad (12b)$$

Experimental geometric specifications of SEGS-LS2 module (Forristall 2003, Dudley *et al.* 1994) and the optical properties are summarised in Table 4 and Table 1, respectively.

The heat losses (Q_{loss}) and efficiency (η) are used in the grid independence test adopting several number of nodes (N) corresponding to different segments sizes ($\Delta l = \frac{L_r}{(N-1)}$). (Q_{loss}) and (η) are computed as follows

$$Q_{loss} = \frac{1}{Aperture} \left[\sum_{i=1}^N (Q_{a-g,i}^{conv} + Q_{a-g,i}^{rad} + Q_{a-bra,i}^{cond}) + \sum_{i=1}^{N-bra} (Q_{a-bra,i}^{conv}) \right] \quad (13)$$

$$\eta = \frac{\dot{m} \cdot \bar{c} (T_{f,N} - T_{f,0})}{I_b \cdot Aperture} \quad (14)$$

Where (\bar{c}) is the HTF specific heat estimated at the arithmetic mean temperature ($\frac{T_{f,N} + T_{f,0}}{2}$), and ($N - bra$) is the number of brackets that support the PTR.

The numerical solution is considered to be grid independent when the change in the efficiency ($E\eta$) and thermal losses (EQ_{loss}) become uniform (unchanged). ($E\eta$) and (EQ_{loss}) are evaluated at each simulation run (k), corresponding to a number of N nodes

$$\left(E\eta = \frac{|\eta^k - \eta^{k-1}|}{\eta^{k-1}} \right) \quad (15)$$

$$\left(EQ_{loss} = \frac{|Q_{loss}^k - Q_{loss}^{k-1}|}{Q_{loss}^{k-1}} \right) \quad (16)$$

For the operating conditions, case 1 in Table 5 is selected in this first series of simulations.

Table 4 Simulations SEGS-LS2 geometric characteristics (Forristall 2003, Dudley *et al.* 1994, Hachicha *et al.* 2013)

Component	Parabolic trough reflector	Absorber	Glass envelope
Geometrical characteristics	$A_{PTC} = w_r \times L_r = 5.0 \text{ m} \times 7.8 \text{ m}$, $f = 1.84 \text{ m}$, $GC = 22.7$	$D_{out}^{abs} = 0.070 \text{ m}$, $D_{inn}^{abs} = 0.066 \text{ m}$ $D_{ptug} = 0.0508 \text{ m}$	$D_{inn}^{glass} = 0.109 \text{ m}$, $D_{out}^{glass} = 0.115 \text{ m}$

Table 5 Various operating conditions implemented in the code for the simulations (Forristall 2003, Dudley *et al.* 1994, Hachicha *et al.* 2013)

case	q_{sun} [$\frac{W}{m^2}$]	HTF \dot{m} [$\frac{m^3}{h}$]	Wind speed [$\frac{m}{s}$]	Air temp. [°C]	HTF in temp. [°C]	HTF out temp. [°C]	Estimated HTF out temp. [°C]	Estimated error [%]
1	933.7	2.862	2.6	21.2	102.2	124	123.766	0.19%
2	968.2	2.868	3.7	22.4	151	173.3	173.322	0.01%
3	982.3	2.946	2.5	24.3	197.5	219.5	219.677	0.08%
4	909.5	3.282	3.3	26.2	250.7	269.4	269.334	0.02%
5	937.9	3.330	1	28.8	297.8	316.9	317.027	0.04%
6	880.6	3.336	2.9	27.5	299	317.2	316.950	0.08%
7	920.9	3.408	2.6	29.5	379.5	398	398.369	0.09%
8	903.2	3.378	4.2	31.1	355.9	374	374.395	0.11%

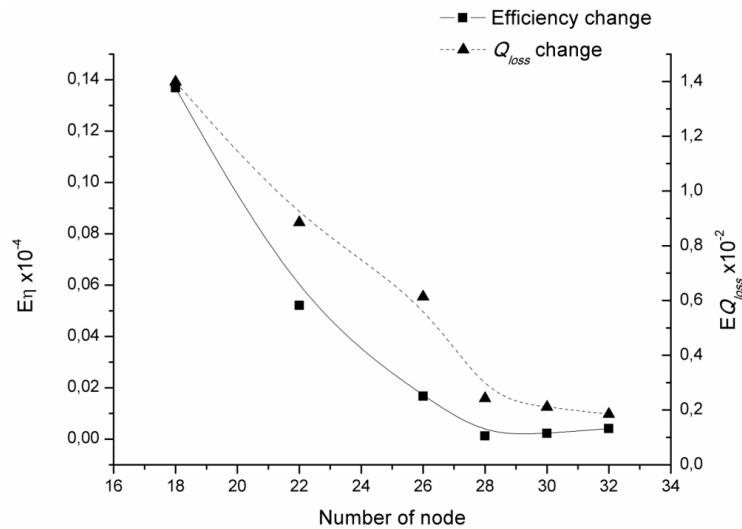


Fig. 6 Efficiency and heat loss changes vs. the number of nodes

Fig. 6 illustrates the evolution of the efficiency changes and heat losses depending on the number of nodes. It is shown that a number $N = 30$ of nodes, corresponding to 29 segments, is enough to state that the solution is not affected by the refinement and is used in the following simulations. Fig. 7 presents comparison of the efficiency numerical results vs experimental data obtained for various operating conditions of Table 5.

The comparison shows a good agreement with a 1.246% root mean square error, while Padilla

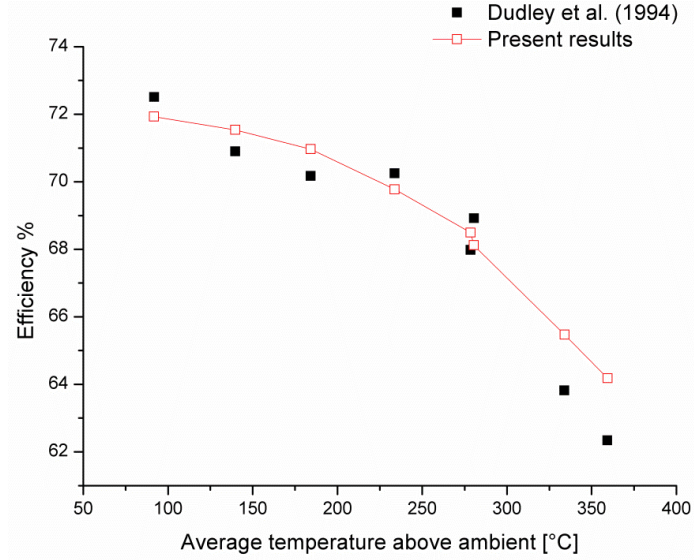


Fig. 7 Efficiency vs. HTF average temperature above ambient $\left(\frac{T_{f,N}+T_{f,0}}{2} + T_{amb}\right)$

et al. (2011), García-Valladares and Velázquez (2009), Forristall (2003) reported 1.012%, 1.433% and 1.382%, respectively. Hachicha *et al.* (2013) reported a mean deviation of 1.25%. The HTF temperature rises through the absorber were compared with experimental measurements (Dudley *et al.* 1994) and were in excellent agreement, with a relative deviation range from 0.01% to 0.19% as presented in Table 5.

Fig. 8 shows the heat loss predicted by the model compared with experimental data of Dudley *et al.* (1994). The heat loss root mean square error was $7.3123 \frac{W}{m^2}$. According to Padilla *et al.* (2011) and Huang *et al.* (2016), results respectively, $10.255 \frac{W}{m^2}$ and $5.68 \frac{W}{m^2}$, the model prediction is good.

3. S-curved receiver versus the CSS receiver

The calibration and validation of the mathematical model were done using SEGS-LS2 experimental data (Dudley *et al.* 1994). Methods, and strategies developed to calibrate the model may be used in other environmental modelling contexts to generate a set of future scenarios on the basis of PTRs new designs.

The first configuration of interest in this study is the CSS receiver in Fig. 3, with the same characteristics used in the validation process without the plug ($D_{plug} = 0$). Within a plain tube, without the plug, the Gnielenski's correlation defined in Eq. (12a) becomes (Incropera *et al.* 2002).

$$\left\{ \begin{array}{l} Nu_{inn,i} = \frac{f_{inn,i}(Re_i - 1000)Pr_{f,i}}{1 + 12.7\sqrt{f_{inn,i}/8}(Pr_{f,i}^{2/3} - 1)} \left(\frac{Pr_{f,i}}{Pr_{a,i}}\right) \\ 0.5 < Pr_{f,i} < 2000, 2300 < Re_i < 5 \cdot 10^6 \end{array} \right. \quad (17)$$

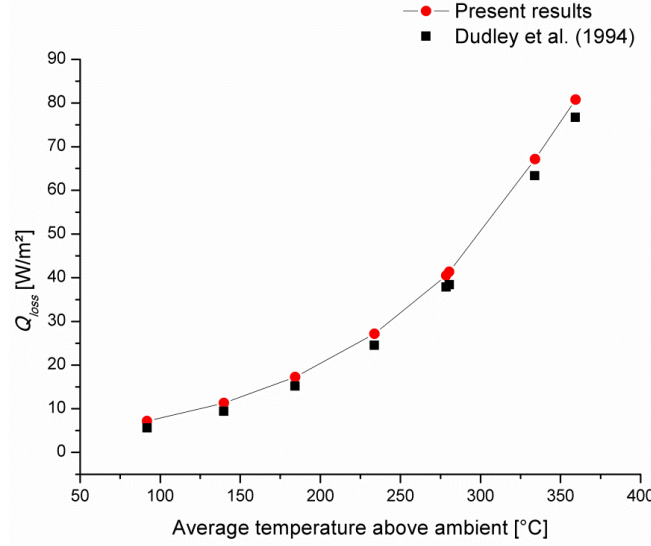


Fig. 8 Heat loss vs. HTF average temperature above ambient $\left[\frac{(T_{f,N} + T_{f,0})}{2} + T_{amb} \right]$

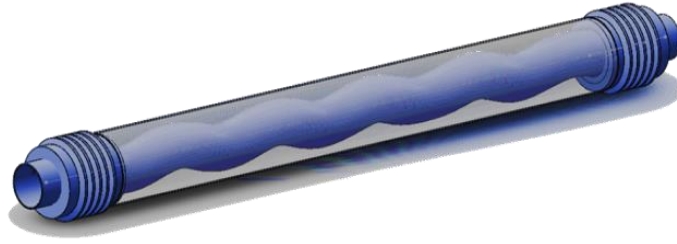


Fig. 9 The novel S-curved receiver according to Demagh *et al.* (2015)

The friction factor ($f_{inn,i}$) for a straight tube is estimated by Colebrook's correlation, as defined in Eq. (12b).

The second solar receiver dealt with in this study was proposed by Demagh *et al.* (2015), as shown in Fig. 9. With an S-curved absorber tube, the inner heat transfer is enhanced (Bitam *et al.* (2018), as well as the concentrated solar radiation on the outer face of the absorber tube is better homogenised (Demagh *et al.* 2015). The main characteristics of the S-curved receiver are: periodic length $\lambda = 195$ mm, peak-to-peak amplitude $2A = 20$ mm, inner pipe diameter $D_i = 66$ mm and the straight length $L_r = 7.8$ m.

Assuming temperature-dependent HTF properties, Bitam *et al.* (2018) validated the numerical results by comparison with experimental correlations of Eqs. (18a)-(18b). The first correlation was used to predict the mean Nusselt number in helically coiled pipes as established by Rogers and Mayhew (1964), and the second by Abou-Arab *et al.* (1991) was used for the mean friction factor.

$$Nu_{inn,i} = 0.023 \cdot Re_i^{0.85} Pr_{f,i}^{0.4} \cdot \delta^{0.1} \quad (18)$$

$$f_{S-curved,i} = f_{inn,i} + 0.0005 \cdot \delta^{0.5} \quad (19)$$

The properties of the HTF are estimated at the arithmetic mean of the inlet and outlet bulk

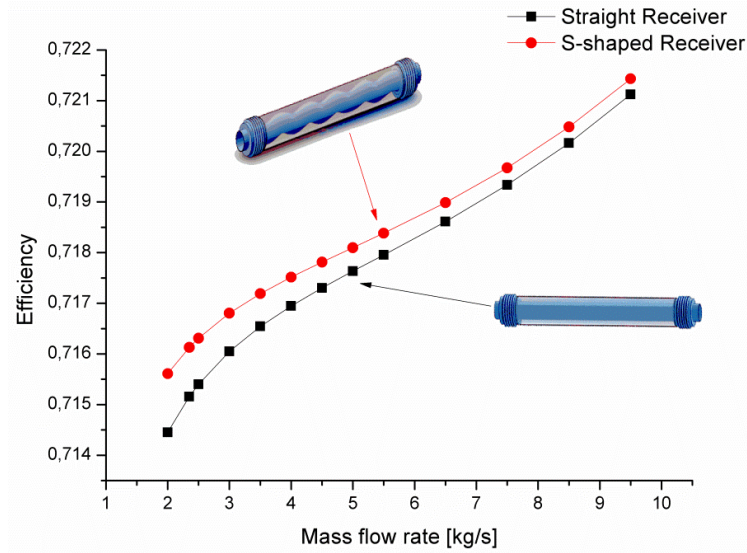


Fig. 10 Improved efficiency of the S-curved receiver

temperatures $\left(\frac{T_{in}+T_{out}}{2}\right)$. The curvature ratio is defined as $\left(\delta = \frac{2\pi^2 \cdot D_i \cdot A}{\lambda^2}\right)$ (Bitam *et al.* 2018, Abou-Arab *et al.* 1991) range is $0.0111 \leq \delta \leq 0.71$.

A comparison with the numerical results of Bitam *et al.* (2018), the correlation by Rogers and Mayhew (1964) (Eq. (18a)) showed a good agreement with a maximum relative error of 5.2%, while for the experimental correlation of Abou-Arab *et al.* (1991) (Eq. (18b)) the maximum relative error was less than 3.9%.

As shown in Figs. 3 and 9, the two configurations of interest in this study are PTRs with a straight and S-curved absorber tubes. Apart from inner tube convective heat transfer coefficient $(Nu_{inn,i})$ of Eq. (5b), all the remaining heat exchanges relations defined in Tables 2(a)-2(b)-2(c) are assumed to be the same for the three configurations of interest, e.g., the SEGS-LS2 receiver (with plug) used in the validation procedure, CSS receiver, and the new S-curved receiver. The expression of the Nusselt number $(Nu_{inn,i})$ of Eq. (5b) is replaced by the correlation (17) obtaining results for the CSS receiver.

While, for the new S-curved receiver, the Nusselt number of Eq. (5b) is replaced by the correlation (18a), and correlation (18b) is used in the Eq. (4) to estimate the pressure drop.

Apart from the HTF inlet temperature $(T_{in} = 450 \text{ K})$, the operating conditions of case 1 as summarised in Table 5 will be used in the following simulations. The comparison between efficiencies is shown in Fig. 10. Despite the use of a rather small absorber (7.8 m length) in the calculations, the new receiver is more efficient than the CSS receiver.

It is noticed that the arc-length of the S-curved receiver tube is longer than the length of the straight tube, about 2.55%. In spite of this fact, the corresponding energy losses through the external face of the absorber tube are lower than those of the CSS receiver as shown in Fig. 11. This result is mainly due to the increase of the heat transfer coefficient (h_{a-f}^{con}) and the decrease of the absorber tube temperature (T_a) . Moreover, Fig. 11 highlighted the convergence of the two curves to a single point for $\dot{m} = 9.50 \frac{\text{kg}}{\text{s}}$, corresponding to a Reynolds number equal to ~ 123000 ; beyond this

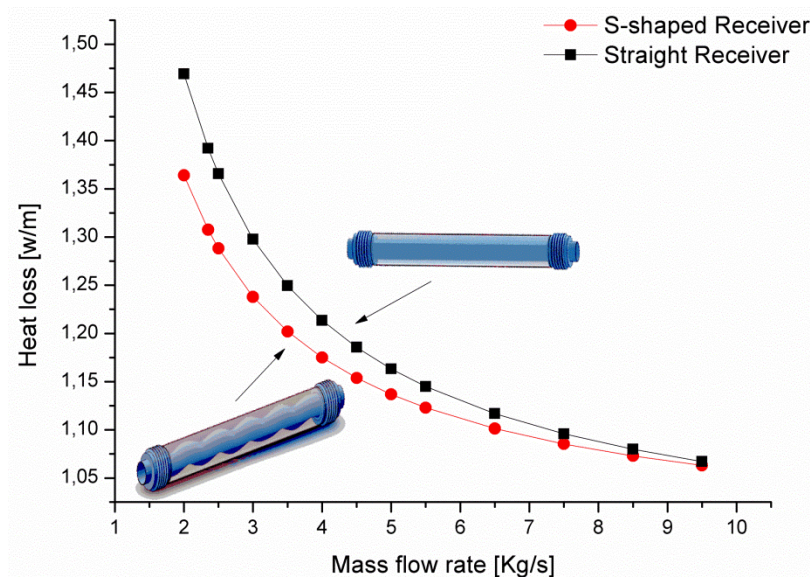


Fig. 11 Reduced heat losses for the S-shaped receiver tube

regime flow, the improvement of heat exchanges inside the solar absorber has almost no influence on heat losses.

4. Conclusions

In this study, a 1-D thermal model based on the first law of thermodynamics was established taking into account the pressure drop and kinetic energy loss effects. The model was validated with LS2-SEGS experimental data and showed a good agreement with a 1.246% root mean square error, which consolidates the neglect of pressure drops and kinetic energy losses in previous models established for CSS receiver. Developed to study contemporary solar receiver designs, the present 1-D thermal model could also be used for the CSS receiver.

Results showed that:

- i. For the S-curved PTR, the increasing of the Nusselt number leads to a slight increase of the pressure drop penalty.
- ii. The use of the S-curved receiver enhances the performance of the parabolic trough module by a maximum of 0.16% compared to the conventional receiver with the same diameter, length and equal flow rates.
- iii. The use of the S-curved receiver drop the thermal losses by a maximum of 7%, corresponding to a mass flow rate of $2 \frac{kg}{s}$. This result is mainly due to the increase in the Nusselt number, and consequently the decreased of the receiver tube outer surface temperature.
- iv. The results showed that from a certain mass flow-rate $\left(9.5 \frac{kg}{s}\right)$ the heat loss of the S-curved receiver remains unchanged despite the improvement in heat transfer.

The developed model and code may be used to evaluate the techniques developed over the last decade to improve PTR performance.

References

- Abou-Arab, T.W., Aldoss, T.K. and Mansour, A. (1991), "Pressure drop in alternating curved tubes", *Appl. Scientif. Res.*, **48**, 1-9. <https://doi.org/10.1007/BF01998662>.
- Bejan, A. (2013), *Convection Heat Transfer*, John Wiley & Sons, Inc., Hoboken, New Jersey.
- Bitam, E., Demagh, Y., Hachicha, A.A., Benmoussa, H. and Kabar, Y. (2018), "Numerical investigation of a novel sinusoidal tube receiver for parabolic trough technology", *Appl. Energy*, **218**, 494-510. <https://doi.org/10.1016/j.apenergy.2018.02.177>.
- Cheng, Z.D., He, Y.L. and Cui, F.Q. (2012), "Numerical study of heat transfer enhancement by unilateral longitudinal vortex generators inside parabolic trough solar receivers", *Int. J. Heat Mass Transf.*, **55**, 5631-5641. <https://doi.org/10.1016/j.ijheatmasstransfer.2012.05.057>.
- Cheng, Z.D., He, Y.L. and Qiu, Y. (2015), "Detailed non uniform thermal model of a parabolic trough solar receiver with two halves and two inactive ends", *Renew. Energy*, **74**, 139-147. <https://doi.org/10.1016/j.renene.2014.07.060>.
- Delgado-Torres, A.M. and García-Rodríguez, L. (2007), "Comparison of solar technologies for driving a desalination system by means of an organic Rankine cycle", *Desalination*, **216**, 276-291. <https://doi.org/10.1016/j.desal.2006.12.013>.
- Demagh, Y., Bordja, L., Kabar, Y. and Benmoussa, H. (2015), "A design method of an S-curved parabolic trough collector absorber with a three dimensional heat flux density distribution", *Solar Energy*, **122**, 873-884. <https://doi.org/10.1016/j.solener.2015.10.002>.
- Demagh, Y., Kabar, Y., Bordja, I. and Noui, S. (2016), "The 3D heat flux density distribution on a novel parabolic trough wavy absorber", *AIP Conf. Proc.*, **1734**, 070004. <https://doi.org/10.1063/1.4949151>.
- Dudley, V., Kolb, G., Sloan, M. and Kearney, D. (1994), "SEGS LS2 solar collector-test results", Tech. Report of Sandia, National Laboratories, SANDIA, 94-1884.
- Forristall, R. (2003), "Heat transfer analysis and modeling of a parabolic trough solar receiver implemented in engineering equation solver", Report NREL.
- Fuqiang, W., Qingzhi, L., Huaizhi, H. and Jianyu, T. (2016), "Parabolic trough receiver with corrugated tube for improving heat transfer and thermal deformation characteristics", *Appl. Energy*, **164**, 411-424. <https://doi.org/10.1016/j.apenergy.2015.11.084>.
- Fuqiang, W., Ziming, C., Jianyu, T., Yuan, Y., Yong, S. and Linhua, L. (2017), "Progress in concentrated solar power technology with parabolic trough collector system: A comprehensive review", *Renew. Sustain. Energy Rev.*, **79**, 1314-1328. <https://doi.org/10.1016/j.rser.2017.05.174>.
- García-Valladares, O. and Velázquez, N. (2009), "Numerical simulation of parabolic trough solar collector: improvement using counter flow concentric circular heat exchangers", *Int. J. Heat Mass Transf.*, **52**(3), 597-609. <https://doi.org/10.1016/j.ijheatmasstransfer.2008.08.004>.
- Ghadirijafarbeigloo, S., Zamzamian, A.H. and Yaghoubi, M. (2014), "3-D numerical simulation of heat transfer and turbulent flow in a receiver tube of solar parabolic trough concentrator with louvered twisted-tape inserts", *Energy Proc.*, **49**, 373-380. <https://doi.org/10.1016/j.egypro.2014.03.040>.
- Gong, G., Huang, X., Wang, J. and Hao, M. (2010), "An optimized model and test of the China's first high temperature parabolic trough solar receiver", *Solar Energy*, **84**, 2230-2245. <https://doi.org/10.1016/j.solener.2010.08.003>.
- Gong, X.K., Wang, F., Wang, H., Tan, J., Lai, Q. and Han, H. (2017), "Heat transfer enhancement analysis of tube receiver for parabolic trough solar collector with pin fin arrays inserting", *Solar Energy*, **144**, 185-202. <https://doi.org/10.1016/j.solener.2017.01.020>.
- Guo, J., Huai, X. and Liu, Z. (2016), "Performance investigation of parabolic trough solar receiver", *Appl. Therm. Eng.*, **95**, 357-364. <https://doi.org/10.1016/j.applthermaleng.2015.11.035>.
- Hachicha, A.A., Rodriguez, I., Capdevila, R. and Oliva, A. (2013), "Heat transfer analysis and numerical simulation of a parabolic trough solar collector", *Appl. Energy*, **111**, 581-592. <https://doi.org/10.1016/j.apenergy.2013.04.067>.
- Huang, W., Xu, Q. and Hu, P. (2016), "Coupling 2D thermal and 3D optical model for performance prediction

of a parabolic trough solar collector”, *Solar Energy*, **139**, 365-380. <https://doi.org/10.1016/j.solener.2016.09.034>.

Huang, Z., Li, Z.Y., Yu, G.L. and Tao, W.Q. (2017), “Numerical investigations on fully-developed mixed turbulent convection in dimpled parabolic trough receiver tubes”, *Appl. Therm. Eng.*, **114**, 1287-1299. <https://doi.org/10.1016/j.applthermaleng.2016.10.012>.

Incropera, F.P. and Dewitt, D.P. (2002), *Fundamentals of Heat and Mass Transfer*, Wiley, New York.

Kalidasan, B., Shankar, R. and Srinivas, T. (2016), “Absorber tube with internal hinged blades for solar parabolic trough collector”, *Energy Procedia*, **90**, 463-469. <https://doi.org/10.1016/j.egypro.2016.11.213>.

Kalogirou, S.A. (2012), “A detailed thermal model of a parabolic trough collector receiver”, *Energy*, **48**, 298-306. <https://doi.org/10.1016/j.energy.2012.06.023>.

Kumar, K.R. and Reddy, K.S. (2009), “Thermal analysis of solar parabolic trough with porous disc receiver”, *Appl. Energy*, **86**(9), 1804-1812. <https://doi.org/10.1016/j.apenergy.2008.11.007>.

Liang, H., You, S. and Zhang, H. (2015), “Comparison of different heat transfer models for parabolic trough solar collectors”, *Appl. Energy*, **148**, 105-114. <https://doi.org/10.1016/j.apenergy.2015.03.059>.

Lu, J., Ding, J., Yang, J. and Yang, X. (2013), “Non uniform heat transfer model and performance of parabolic trough solar receiver”, *Energy*, **59**, 666-675. <https://doi.org/10.1016/j.energy.2013.07.052>.

Muñoz, J. and Abánades, A. (2011), “Analysis of internal helically finned tubes for parabolic trough design by CFD tool”, *Appl. Energy*, **88**(11), 4139-4149. <https://doi.org/10.1016/j.apenergy.2011.04.026>.

Mwesigye, A., Bello-Ochende, T. and Meyer, J.P. (2014), “Heat transfer and thermodynamic performance of a parabolic trough receiver with centrally placed perforated plate inserts”, *Appl. Energy*, **136**, 989-1003. <https://doi.org/10.1016/j.apenergy.2014.03.037>.

Padilla, R.V., Demirkaya, G., Goswami, D.Y., Stefanakos, E. and Rahman, M.M. (2011), “Heat transfer analysis of parabolic trough solar receiver”, *Appl. Energy*, **88**, 5097-5110. <https://doi.org/10.1016/j.apenergy.2011.07.012>.

Reddy, K.S., Kumar, K.R. and Ajay, C.S. (2015), “Experimental investigation of porous disc enhanced receiver for solar parabolic trough collector”, *Renew. Energy*, **77**, 308-319. <https://doi.org/10.1016/j.renene.2014.12.016>.

Rogers, G.F.C. and Mayhew, Y.R. (1964), “Heat transfer and pressure loss in helically coiled tubes with turbulent flow”, *Int J Heat Mass Transf.*, **7**, 1207-1216. [https://doi.org/10.1016/0017-9310\(64\)90062-6](https://doi.org/10.1016/0017-9310(64)90062-6).

Wang, P., Liu, D.Y. and Xu, C. (2013), “Numerical study of heat transfer enhancement in the receiver tube of direct steam generation with parabolic trough by inserting metal foams”, *Appl. Energy*, **102**, 449-460. <https://doi.org/10.1016/j.apenergy.2012.07.026>.

CC

Nomenclature

$A[m], [m^2]$	Amplitude of the sinusoid, or area
a, b	Accommodation and interaction coefficients
$c[J \cdot kg^{-1} \cdot K^{-1}]$	HTF specific heat
$D[m]$	Diameter
$E\eta[-]$	Change in the efficiency
$E Q_{loss}[-]$	Change in the heat loss
$f[-], [m]$	Friction factor, or focal length
$f_{inn}[-]$	Friction factor
$h[W \cdot m^{-2} \cdot K^{-1}]$	Heat transfer coefficient
$k[cm]$	Mean-free-path between molecule collisions (cm)
$\Delta l[m]$	Segment length

$\dot{m}[\text{kg} \cdot \text{s}^{-1}]$	Mass flow rate
$N[-]$	Segments number
$Nu[-]$	Nusselt number
$P[N \cdot \text{m}^{-2}]$	Pressure
$P_{bra}[m]$	Perimeter of bracket
Pr	Prandtl number
$\Delta P _i[N \cdot \text{m}^{-2}]$	Pressure drop through the segment i
$Q[W]$	Mean heat flux
$q_{sun}[W \cdot \text{m}^{-2}]$	Direct Solar Insolation
$r[-]$	Diameters ratio
$Ra[-]$	Rayleigh number
Re	Reynolds number
$T[K]$	Temperature
$T_f[K]$	HTF film temperature
$T_{base}[K]$	Temperature at base of bracket
$V[\text{m} \cdot \text{s}^{-1}]$	HTF velocity
$u[J \cdot \text{kg}^{-1}]$	Specific internal energy
$L_r[m]$	Straight length of the receiver

Greek Letters

$\alpha[-]$	Absorptance
$\gamma[-]$	Ratio of specific heats
$\delta[-], [\text{cm}]$	Curvature ratio, molecular diameter of annulus gas (cm)
$\varepsilon[-], [= 1.5 \cdot 10^{-6}\text{m}]$	Emittance, equivalent roughness
$\eta[-]$	Efficiency
$\kappa[-]$	Incident angle modifier
$\lambda_{std}[W \cdot \text{m}^{-1} \cdot \text{K}^{-1}]$	Thermal conductance of the annulus gas at standards temperature and pressure
$\lambda[m], [W \cdot \text{m}^{-1} \cdot \text{K}^{-1}]$	Periodicity length, or thermal conductivity
$\rho[\text{kg} \cdot \text{m}^{-3}], [-]$	Density, reflectivity (reflectance)
$\sigma = 5.670373 \times 10^{-8}$ $[W \cdot \text{m}^{-2} \cdot \text{K}^{-4}]$	Stefan-Boltzmann constant
$\tau[-]$	Transmittance

Subscripts

A	Absorber tube
Amb	Ambient
bra	Bracket
cs	Cross-section of the tube
f	HTF
g	Glass envelope
i	Segment subscript
inn and out	Inner and outer faces
in and out	Absorber tube inlet and outlet
opt	Optical
r	Receiver

Superscripts

<i>Abs</i>	Absorber tube
<i>Conv</i>	Convective heat transfer
<i>Glas</i>	Glass envelope
<i>Cond</i>	Conduction heat transfer
"	Initial field condition
<i>Rad</i>	Radiation heat transfer

Abbreviations

<i>CFD</i>	Computational Fluid Dynamics
<i>CSS</i>	Conventional straight and smooth
<i>HTF</i>	Heat transfer fluid
<i>PTC</i>	Parabolic Trough Collector
<i>PTR</i>	Parabolic Trough Receiver